INTERNATIONAL JOURNAL FOR NUMERICAL METHODS IN FLUIDS
Int. J. Numer. Meth. Fluids **31**: 767–785 (1999)

NUMERICAL STUDY OF TURBULENT FLOW OVER TWO-DIMENSIONAL SURFACE-MOUNTED RIBS IN A CHANNEL

ROBERT R. HWANG[a,*], Y.C. CHOW[b] AND Y.F. PENG[a]

[a] *Institute of Physics, Academia Sinica, Nankang, Taipei 11529, Taiwan, Republic of China*
[b] *Department of Naval Architecture and Ocean Engineering, Taipei 10764, Taiwan, Republic of China*

SUMMARY

This study accurately predicts the cases of turbulent flow around a surface-mounted two-dimensional rib with varying lengths. The numerical method employs a differencing scheme for integrating the elliptic Reynolds-averaged Navier–Stokes equations and the continuity equation. A two-equation k–ε turbulence model is employed to simulate the turbulent transport quantities and close the solving problem. The near-wall regions of the separated sides of the rib are resolved by a near-wall model of a two-layer approach instead of the wall function approximation. Computations for flow over a surface-mounted rectangular rib are conducted for the variations in the rib lengths. Results indicate that upstream of the obstacle, the length of the recirculating region remains unchanged with varying rib lengths; while the downstream length of the recirculating region is a strong function of rib length and changes nearly linearly for the varying lengths of $B/H = 0.1$ to $B/H = 4.0$. Reattachment on top of the rib, owing to its increasing length, affects the downstream boundary layer development. Copyright © 1999 John Wiley & Sons, Ltd.

KEY WORDS: turbulent flow; surface-mounted rib; channel flow; numerical study

1. INTRODUCTION

Flows including separation and reattachment frequently occur in many engineering problems. These flows can be observed in wind engineering and many fluid devices, such as weirs, gas turbines, turbomachines and combustion ducts. Despite their frequent appearance in engineering, the study of them is still limited due to the complexities and difficulties encountered. The flow around a surface-mounted obstacle constitutes two basic study cases for strongly separated flows occurring both upstream and downstream of the obstacle. The basic characteristic of such flow configurations is the integral parameters of the length of the recirculating region afore and behind the obstacle. These lengths depend on the ratio of the boundary layer thickness of the approaching flow to the obstacle height and also the geometry of the obstacle itself.

Numerous investigations have been conducted to examine such a turbulent flow around two-dimensional surface-mounted ribs. In the experiments, Bergeles and Athanassiadis [1] measured the lengths of the recirculating regions afore and behind the obstacle. Antoniou and

* Correspondence to: Institute of Physics, Academia Sinica, Nankang, Taipei 11529, Taiwan, Republic of China. Fax + 886 2 27834187; e-mail: phhwang@ccvax.sinica.edu.tw

CCC 0271–2091/99/200767–19$17.50

Received January 1998
Revised March 1998

Bergeles [2] measured the mean velocity and turbulence intensity along with integral properties of the developing flow to examine the region behind a two-dimensional surface-mounted prism of varying length after reattachment. In using a conventional fiber optic laser-Doppler anemometer (LDA) system, Acharya *et al.* [3] measured the flow of mean velocities and Reynolds stresses in the upstream and downstream recirculating regions of a separated duct flow past a two-dimensional surface-mounted square rib. In the numerical investigations, most of the studies attempted to improve the turbulence models to simulate the turbulent transported quantities. It included the studies of Acharya *et al.* [3], Durst and Rastogi [4] and Benodekar *et al.* [5]. To account for the near-wall effects in using the non-linear $k-\varepsilon$ model to simulate the turbulence quantities, the wall function approximations are used in these studies. Predicted results indicated that all the models underpredict the magnitude of the mean velocities and Reynolds stresses in the near-wall regions of the separated sides.

In consideration of the flow parallel to the wall and equilibrium relations, the use of the wall function for the near-wall treatment is correct only for simple shear flows. As mentioned previously, flow past a surface-mounted rib exists as strongly separated flows around the obstacle. Hence, a certain error is created when the wall function approach is applied to predict such complex wall shear flows. An alternative to the use of wall functions is to employ turbulence models that are valid all the way to the wall. In recent years, many researchers have tried to develop low-Reynolds number models by incorporating either a wall damping effect or a direct effect of molecular viscosity or both in the empirical constants and functions in the turbulence transport equations, derived originally for high-Reynolds number, fully turbulent flows far from the wall. Several low-Reynolds number models have been reviewed by Patel *et al.* [6] and Michelassi and Shih [7]. Previous calculations indicated that the damping functions developed for attached boundary layers are not always well behaved in separated flows.

In order to save grid points and hence computer storage and time comparing low-Reynolds number models, and also to introduce the fairly well-established length scale distribution very near the walls into the turbulence model, the use of a two-layer approach becomes more effective. In the two-layer approach the near-wall viscosity affected regions are resolved, where the dissipation rate of the turbulent kinetic energy ε is determined by a prescribed length scale distribution l_ε instead of by the transport differential equation. A variety of two-dimensional boundary layer flows and separated flows have been tested with two-layer models, e.g. adverse pressure gradient boundary layer flows [8] and flows with secondary reversed flow [9,10]. It is found that two-layer models can predict more promising results than the wall function approach. Hence, it is concluded that two-layer models are promising tools for practical applications in flows where wall function approximations are either not applicable or inaccurate. The main objectives of the present study are, therefore, to assess the ability of the standard $k-\varepsilon$ turbulence model in coupling with the framework of the two-layer approach to predict the flow behaviour and to investigate the flow past a surface-mounted prism with varying lengths.

2. MATHEMATICAL FORMULATION

2.1. Governing equations

As Figure 1 schematically shows, the physical problem considered in this study is a turbulent conduct flow over a surface-mounted, two-dimensional rectangular rib with varying lengths. The governing Reynolds-averaged equations for steady state turbulent flow of a two-dimensional incompressible fluid are

Continuity:

$$\frac{\partial U}{\partial X}+\frac{\partial V}{\partial Y}=0, \tag{1}$$

Momentum:

$$U\frac{\partial U}{\partial X}+V\frac{\partial U}{\partial Y}=-\frac{1}{\rho}\frac{\partial P}{\partial X}+\frac{\partial}{\partial X}\left(v\frac{\partial U}{\partial X}\right)+\frac{\partial}{\partial Y}\left(v\frac{\partial U}{\partial Y}\right)+\frac{\partial}{\partial X}(-\overline{uu})+\frac{\partial}{\partial Y}(-\overline{uv}), \tag{2}$$

$$U\frac{\partial V}{\partial X}+V\frac{\partial V}{\partial Y}=-\frac{1}{\rho}\frac{\partial P}{\partial Y}+\frac{\partial}{\partial X}\left(v\frac{\partial V}{\partial X}\right)+\frac{\partial}{\partial Y}\left(v\frac{\partial V}{\partial Y}\right)+\frac{\partial}{\partial X}(-\overline{uv})+\frac{\partial}{\partial Y}(-\overline{vv}), \tag{3}$$

where (U, V) and (u, v) denote the mean velocity components and the fluctuating velocity components in the (X, Y) directions respectively, P represents the mean pressure, v is the molecular kinematic viscosity and $(\overline{uu}, \overline{uv}, \overline{vv})$ are the Reynolds stresses.

2.2. Turbulence models

To solve Equations (1)–(3), a turbulence model for the turbulent transport quantities has to be specified. Herein, the standard k–ε model [11] based on the Boussinesq approximation is adopted. The local mean state of turbulence can be characterized by the turbulent kinetic energy k and its dissipation rate ε according to

$$-\overline{u_i u_j}=v_t\left(\frac{\partial U_i}{\partial X_j}+\frac{\partial U_j}{\partial X_i}\right)-\frac{2}{3}\delta_{ij}k, \tag{4}$$

with

$$v_t=C_\mu k^2/\varepsilon. \tag{5}$$

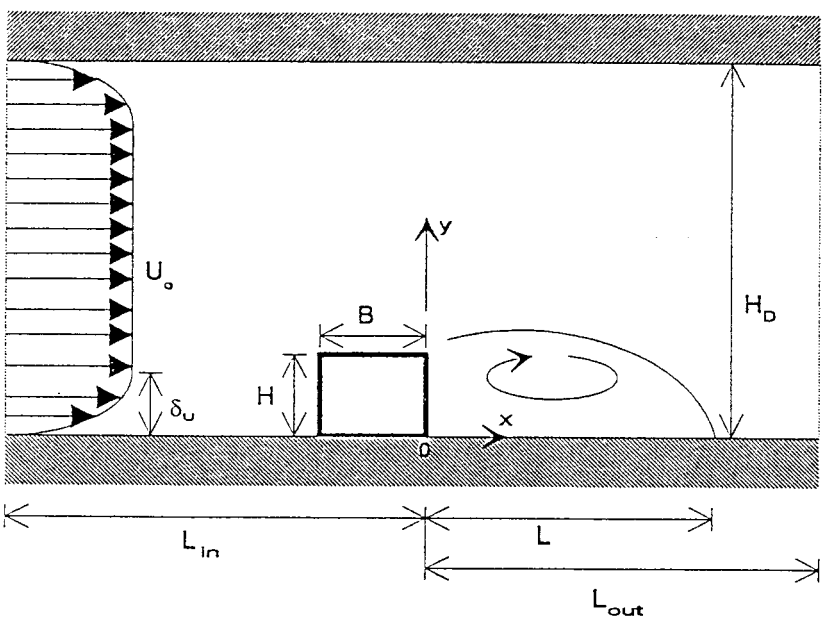

Figure 1. The considered flow problem.

The equations for k and ε can be written as

$$U_j \frac{\partial k}{\partial X_j} = \frac{\partial}{\partial X_j}\left(\frac{v_t}{\sigma_k}\frac{\partial k}{\partial X_j}\right) + G - \varepsilon, \tag{6}$$

$$U_j \frac{\partial \varepsilon}{\partial X_j} = \frac{\partial}{\partial X_j}\left(\frac{v_t}{\sigma_\varepsilon}\frac{\partial \varepsilon}{\partial X_j}\right) + C_1 \frac{\varepsilon}{k} G - C_2 \frac{\varepsilon^2}{k}, \tag{7}$$

where

$$G = v_t \frac{\partial U_i}{\partial X_j}\left(\frac{\partial U_i}{\partial X_j} + \frac{\partial U_j}{\partial X_i}\right).$$

σ_k, σ_ε, C_μ, C_1 and C_2 are modelling coefficients given as follows:

C_μ	σ_k	σ_ε	C_1	C_2
0.09	1.0	1.3	1.44	1.92

To account for the near-wall effects in the standard k–ε model, a two-layer approach is used. In the viscosity affected regions near the wall of the separated regions, these turbulent equations were modified analytically to resemble the near-wall approach method of Chen and Patel [8]. The turbulent eddy viscosity v_t is determined by

$$v_t = C_\mu k^{1/2} l_\mu, \tag{8}$$

and ε is determined from

$$\varepsilon = k^{3/2}/l_\varepsilon. \tag{9}$$

The length scales l_μ and l_ε are adopted as follows:

$$l_\mu = C_3 y[1 - \exp(-R_y/A_\mu)], \tag{10}$$

$$l_\varepsilon = C_3 y[1 - \exp(-R_y/A_\varepsilon)], \tag{11}$$

where both length scales contain damping effects in the near-wall region in terms of the turbulence Reynolds number $R_y = k^{1/2} y/v$. Here y is the normal distance from the wall. The turbulence model moduli are given as $C_3 = \kappa C_\mu^{3/4}$, $A_\varepsilon = 2C_3$ and $A_\mu = 70$, where κ is the Karman constant and $C_\mu = 0.09$.

In conducting the computation, the flow domain is divided into two regions. Region I includes the sublayer, the buffer layer and part of the fully turbulent layer. A one-equation model is employed in this region to account for the wall proximity effects. In region II, beyond the near-wall layer, the standard k–ε model is employed to calculate the velocity field as well as the eddy viscosity. The matching between the one-equation model and the model used further away from the wall should be effective near the viscous sublayer edge, where viscosity effects become small. For fully turbulent boundary layers this corresponds to the order of $y^+ \sim 100$. For good near-wall resolution, the first grid point should be located at $y^+ \sim 1$ and 15 grids are set across to the near-wall layer in the computation of the near-wall boundary. When the viscous sublayer is resolved with the one-equation model, the no-slip conditions are used as boundary conditions.

2.3. Boundary conditions

Figure 1 presents the flow of the calculation domain. The inlet boundary is located at 15 rib heights upstream of the obstacle. To compare the results with experimental data of Acharya *et al.* [3], their inlet flow conditions were used for the specification.

$$\frac{U}{U_0}=\left(\frac{y}{\delta_u}\right)^{1/5.6} \quad \text{if} \quad \frac{y}{\delta_u}<1 \qquad \text{and} \quad \frac{y}{\delta_u}>\left(\frac{H_D}{\delta_u}-1\right),$$

$$\frac{U}{U_0}=1 \qquad \text{if} \quad 1\le\frac{y}{\delta_u}\le\left(\frac{H_D}{\delta_u}-1\right),$$

$$V_0=0, \quad k_0=0.008U_0^2, \quad \varepsilon_0=k^{1.5}/H,$$

where the boundary layer thickness, $\delta_u=3.3H$ and $H_D=9.5H$.

The outlet boundary conditions are specified at a location of 20 rib heights downstream of the obstacle. There, the normal gradients of the mean velocities and turbulent quantities are taken to be zero. No-slip boundary conditions are imposed along the fixed walls and the boundary conditions are specified as $U=V=k=0$.

3. COMPUTATIONAL DETAILS

3.1. Numerical techniques

This study indicates that the numerical computations were performed on a non-uniform and staggered marker and cell (MAC) grid system. In the staggered grid system, the pressure and other dependent scalar variables, such as k and ε, are calculated at nodal points of the mean velocity.

To solve the partial differential equations (1)–(7), which are of an elliptic type, a computer code based on the power law difference (PLD) method [12] is constructed for use in the present study. Briefly, the convection and diffusion terms of the transport equation for ϕ ($\phi=U, V, k, \varepsilon$), i.e.

$$\frac{\partial(U_j\phi)}{\partial X_j}=\frac{\partial[\Gamma(\partial\phi/\partial X_j)]}{\partial X_j}+S_\phi,$$

are discretized by the PLD and the source term by the second-order central differencing, and then integrated within a control volume element to obtain an algebraic equation. The pressure field P is solved with the SIMPLEC algorithm of Van Doormaal and Raithby [13]. The linear algebraic equation system is solved by the alternating direction line by line iteration method. The convergence criterion is specified as the relative difference of every dependent variable between iteration steps being smaller than 10^{-4}. The computations were performed on a Pentium-pro 200 PC. It takes 20000 iterations and 4 h of CPU time to obtain a steady solution with grids of 139×86.

3.2. Grid independence studies

Numerical experiments have also been conducted to determine an adequate grid distribution for this study. Two grid distributions, (139, 86) and (250, 150), are used to conduct the

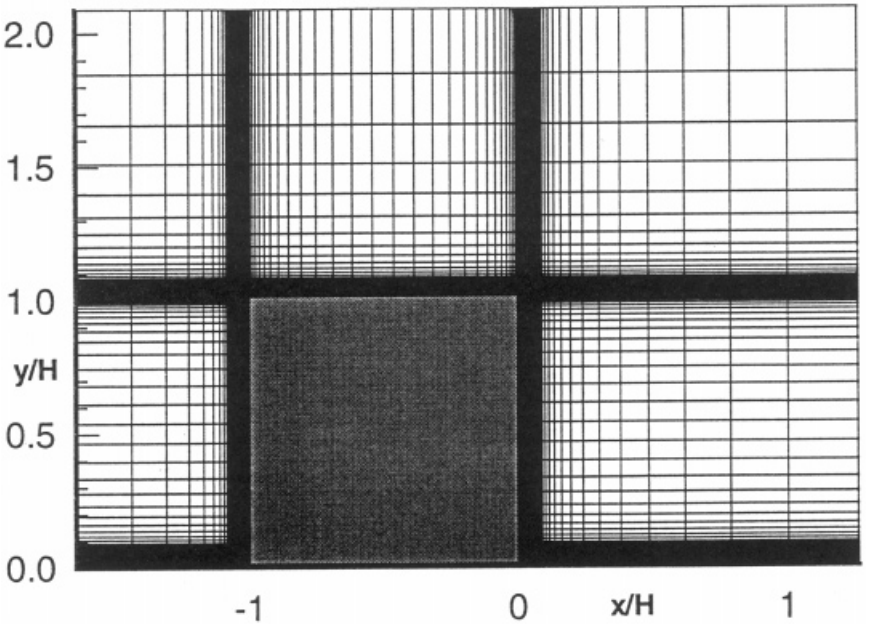

Figure 2. The arrangement of the computation grids near the rib.

computations for the case of turbulent flow over a surface-mounted two-dimensional square rib. In all cases, the grid points were non-uniformly distributed using a power law expression of an automatic mesh generator used by Nichols *et al.* [14] in such that the mesh in the x- and y-directions was packed toward the rib. Figure 2 presents the arrangement of the grid mesh near the rib. The reattachment lengths behind the rib predicted by the present model on the (139, 86) and (250, 150) meshes were within 6% of each other. On the mean velocity prediction of the x component at four sections of $X/H = -1.4,\ -0.5$, 3.8 and 7.1, the profiles of the mean velocity distribution on the (139, 86) and (250, 150) meshes were found to be similar. Therefore, results herein are considered to be grid-independent. Grid sizes of computations adopted in this study are varied with cases of different length to height ratios of rib and indicated as follows:

B/H	0.1	0.5	1.0	2.0	4.0
$(N_x \times N_y)$	127×86	139×86	139×86	143×86	146×86

4. RESULTS AND ANALYSIS

4.1. Test case

To test the accuracy and validity of the numerical computations, a case of a turbulent duct flow over a surface-mounted two-dimensional square rib ($B/H = 1$) is computed and compared with the previous study of Acharya *et al.* [3]. Table I shows all relevant parameters in the experiments of Acharya *et al.* [3] and the corresponding values used in present model. Computational results are presented for those quantities reported. The first consideration is to

predict the gross parameters of the flow fields, among which the reattachment length is a sensitive parameter that has been historically used to assess the overall predictive ability. In the experimental study of Acharya *et al.* [3], reattachment occurs at $L/H = 6.3 \pm 0.9$, while the reattachment length predicted in this study is $L/H = 6.9$. It indicates that the prediction of the current study is within the experimental uncertainty.

To compare the predicted results with the related study, profiles of the U, V, $\overline{uu}$, $\overline{vv}$, $\overline{uv}$ are plotted for several stations at upstream, top surface and downstream of the rib. In Figures 3 and 4, the computed mean velocity of profiles U and V are compared with the experimental data of Acharya et al. [3], and also their predicted results. The finding indicates that the near-wall treatments by the two-layer approach do improve the prediction better than that predicted by the wall function in the near-wall region at a station above and downstream of the rib. At the station $x/H = -1.4$ upstream of the rib, both models underpredict the magnitude of the velocity in the stagnant region when compared with the measurements. The reason may be as stated by Rodi [15] that, in stagnation flows, the turbulent energy production is mostly due to normal stresses rather than shear stresses. It may then cause the prediction to have such a significant deviation in the upstream stagnant region using an isotropic eddy viscosity model. A turbulence model can account for better anisotropic effects and consequently the energy productions may lead to improving the computational results in the front region of the rib.

Figures 5–7 depict respectively, the computed profiles of $(\overline{uu})^{1/2}$, $(\overline{vv})^{1/2}$ and $(\overline{uv})^{1/2}$ compared with the experimental data of Acharya *et al.* [3]. Predicted results by the two-layer approach apparently fit better with the experimental data in the near-wall region than that predicted by the wall function treatment. Hence, the standard k–ε turbulence model encountered with the near-wall treatment of two-layer approach can be an effective model to examine the flow problem of the turbulent flow past a surface-mounted rib.

4.2. Rib of varying lengths

Flow past a surface-mounted rib with varying lengths has been conducted for five cases, namely $B/H = 0.1$, 0.5, 1.0, 2.0 and 4.0. Figure 8 presents the calculated streamline contours for flow past a rib with varying lengths. It can be seen that the flow passes over the prism and then reattaches downstream. The horizontal distance from the downstream rib side to the reattachment point is called the recirculating length (or the reattachment length). At the upstream side of the rib, an upstream recirculating region also occurred owing to the blockage of the rib. It is found that upstream of the obstacle, the lengths of the main recirculating region are nearly identical at varying lengths of the rib; however, the downstream length of the recirculating region is a strong function of the length of rib. Figure 9 depicts the length of the downstream recirculating region L/H in the variations of the rib length, B/H with respect to the rib height. It indicates that L/H changes almost linearly from 7.9 for $B/H = 0.5$ to 4.8 for $B/H = 4.0$. Restated, increasing the length of the obstacle decreases the length of the

Table I. Relevant dimensional and non-dimensional parameters (in SI units)

Parameters	U_0	δ_u	H	B	H_D	ν	L_{in}	L_{out}	$Re = U_0 \times H_D/\nu$
Experimental data [3]	3.6	0.02096	0.00635	0.00635	0.061	1.57E−5	0.095	0.191	14 000
Present study	3.6	0.02096	0.00635	0.00635	0.061	1.57E−5	0.095	0.127	14 000

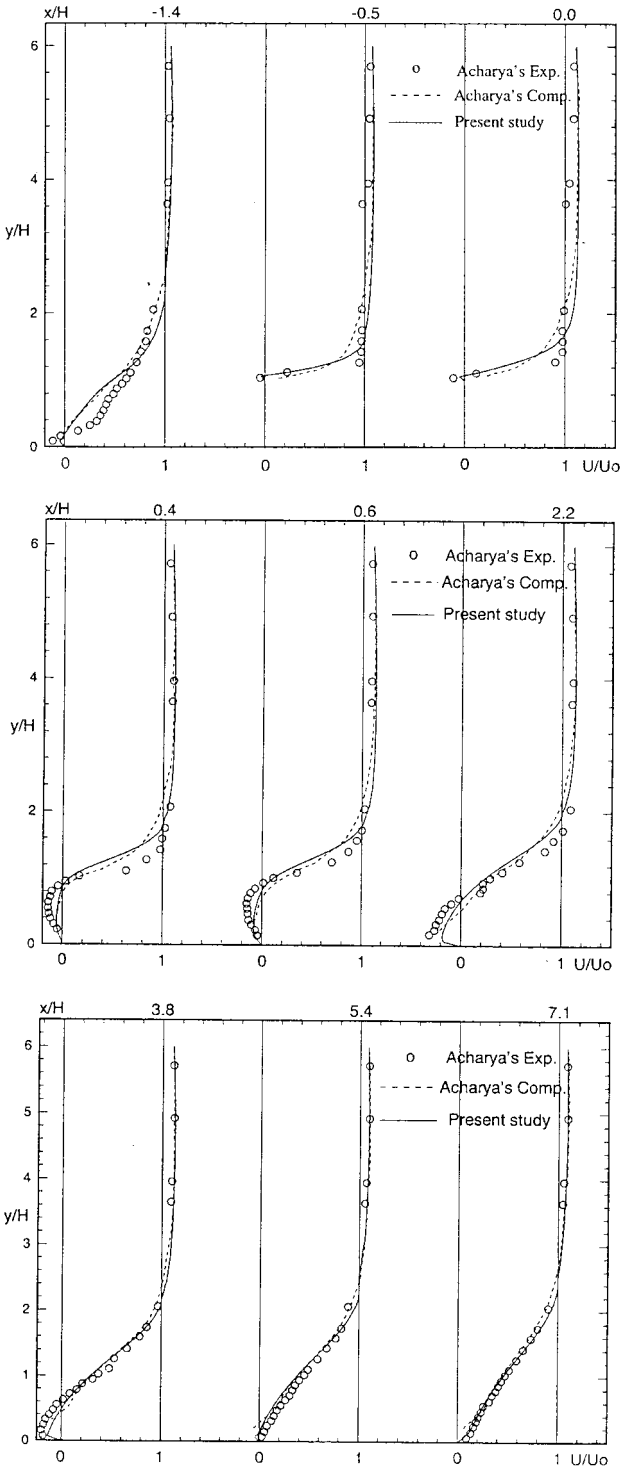

Figure 3. U/U_0 at different streamwise locations for the case of $B/H = 1$.

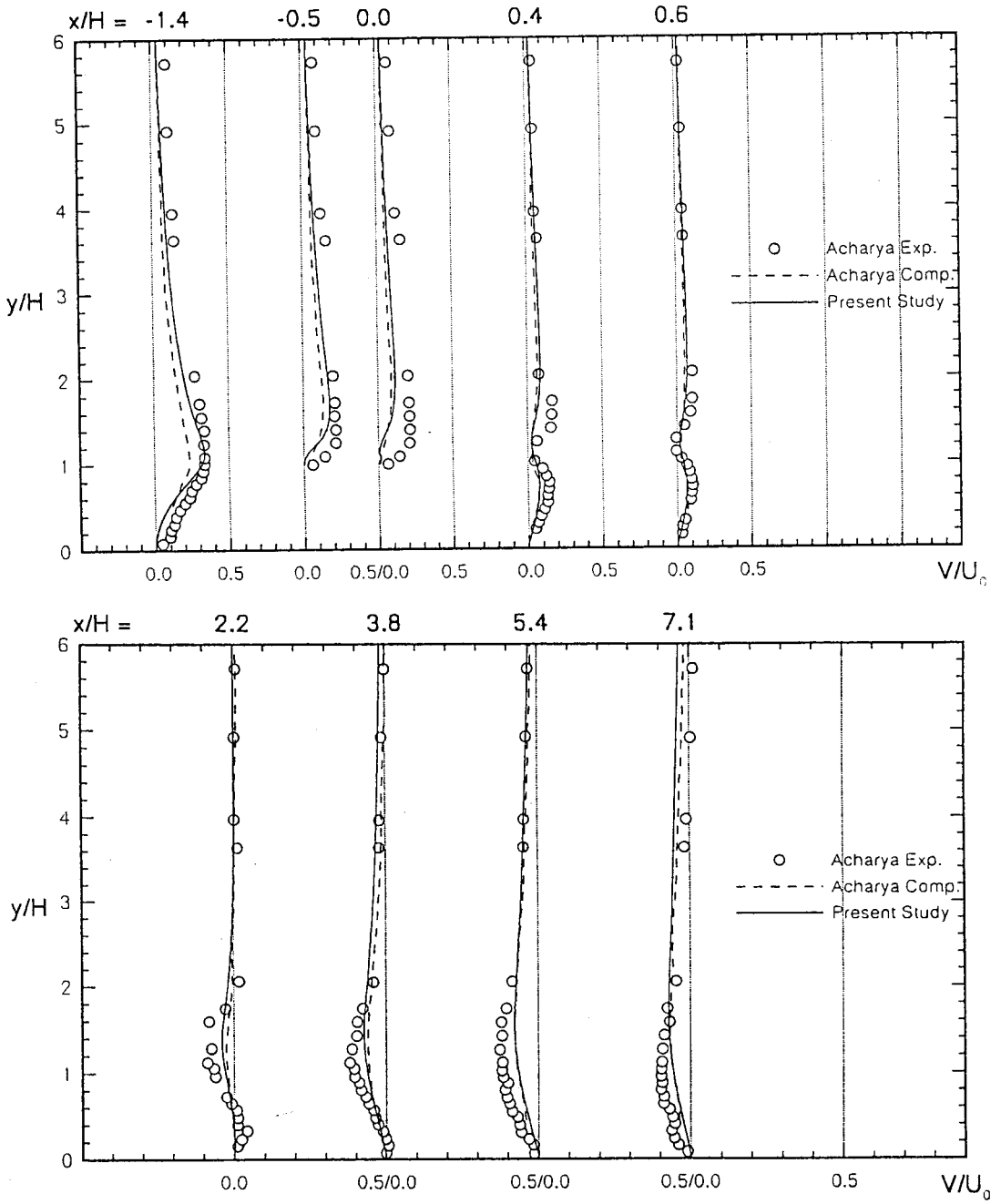

Figure 4. V/U_0 at different streamwise locations for the case of $B/H = 1$.

recirculating region downstream. Also conducted was a case with $B/H = 5.0$, the length of the recirculating region downstream obtained is nearly the same as the case of $B/H = 4.0$. For the case of $B/H = 4.0$, the flow separates from the upstream leading-edge of the obstacle and reattaches on the top surface of the obstacle where part of it is deflected upwards entering into

the recirculating region located on the top of the surface while the other moves downstream. It thus proves that after the flow reattachment on the top surface of the obstacle, the length of the recirculating region downstream remains nearly unchanged irrespective of the obstacle length. This is similar to the experimental study of Bergeles and Athanassiadis [1].

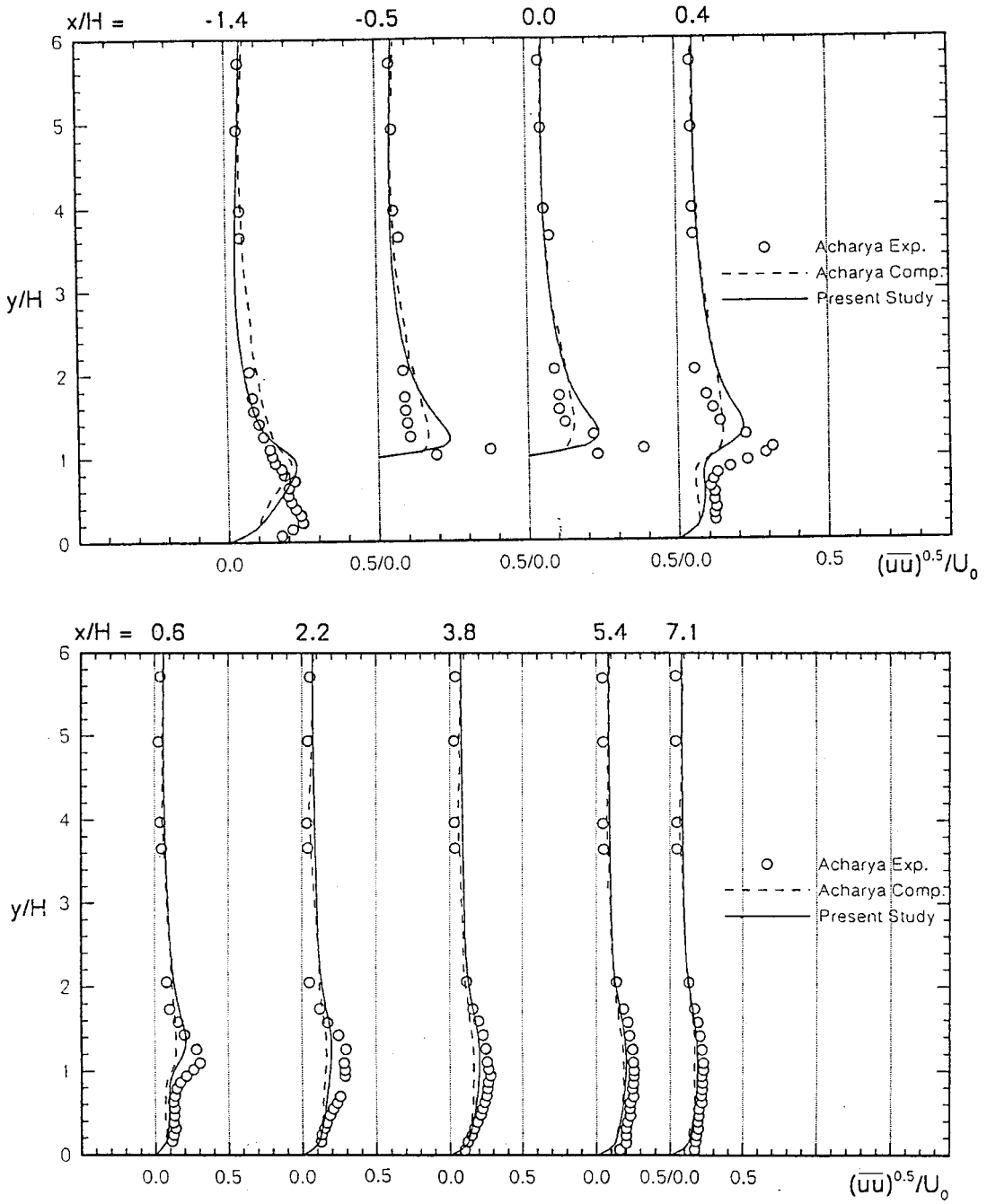

Figure 5. $(\overline{uu})^{1/2}/U_0$ at different streamwise locations for the case of $B/H = 1$.

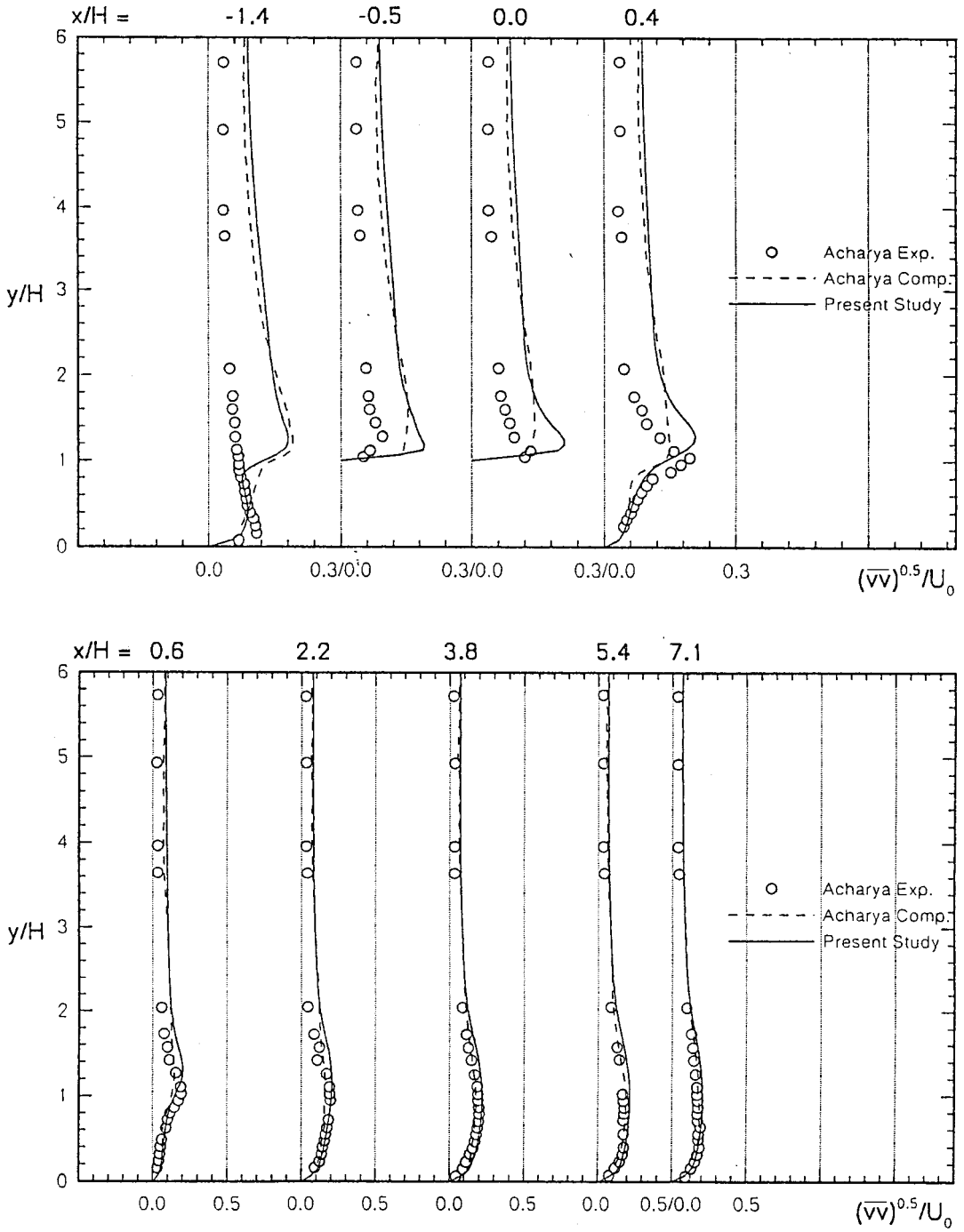

Figure 6. $(\overline{vv})^{1/2}/U_0$ at different streamwise locations for the case of $B/H = 1$.

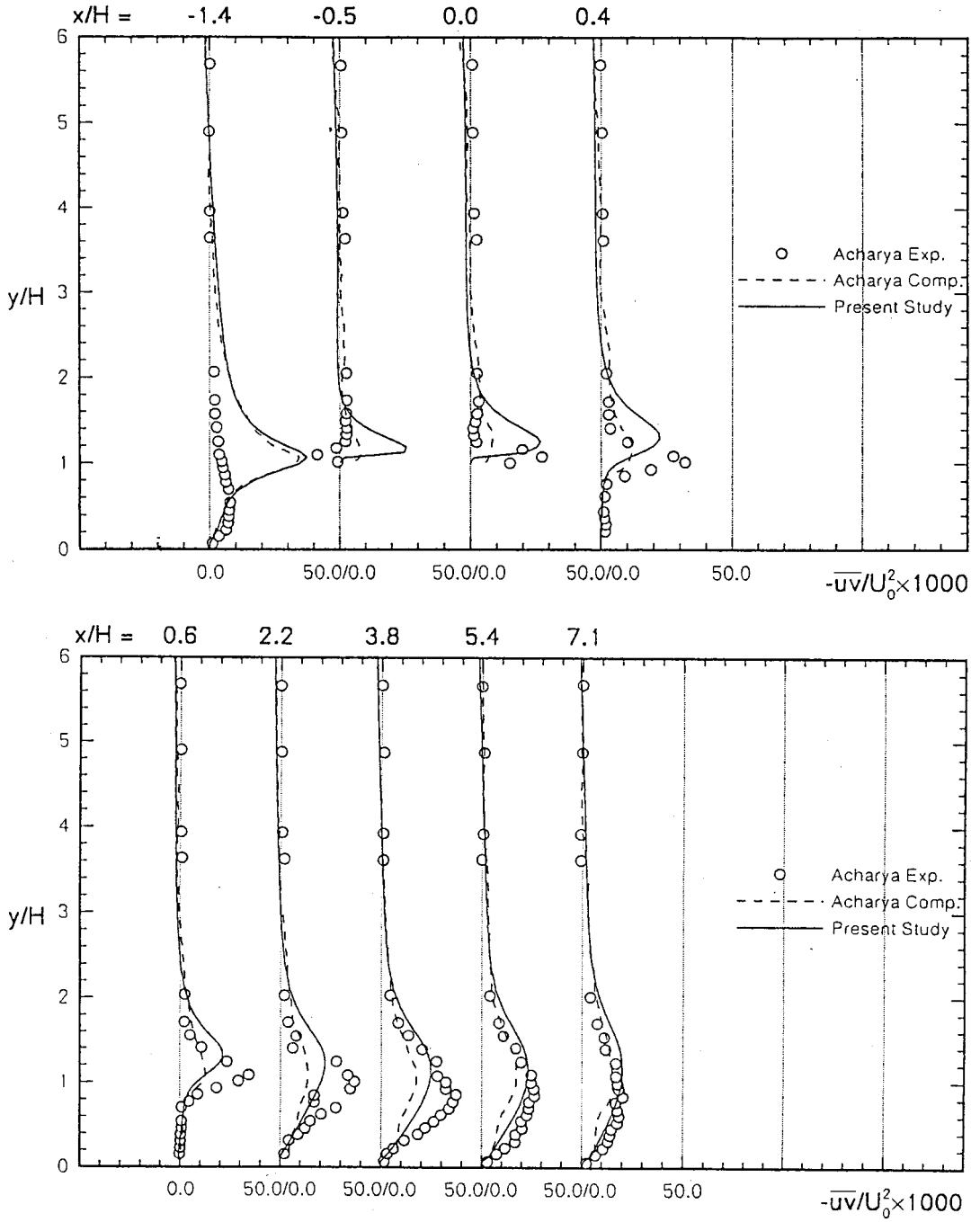

Figure 7. $(\overline{uv})^{1/2}/U_0$ at different streamwise locations for the case of $B/H = 1$.

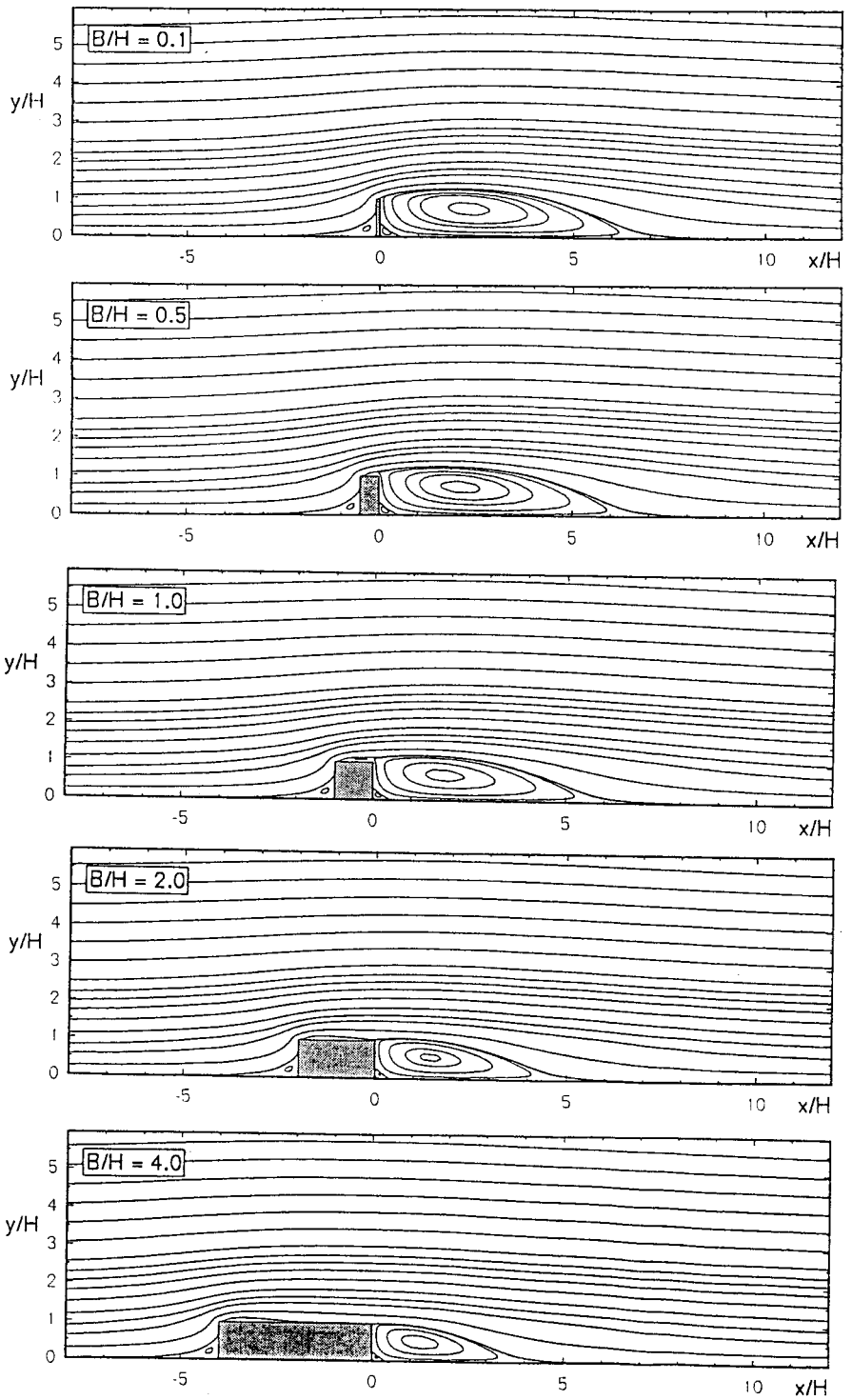

Figure 8. Streamfunction contours for flow over rib with varying length.

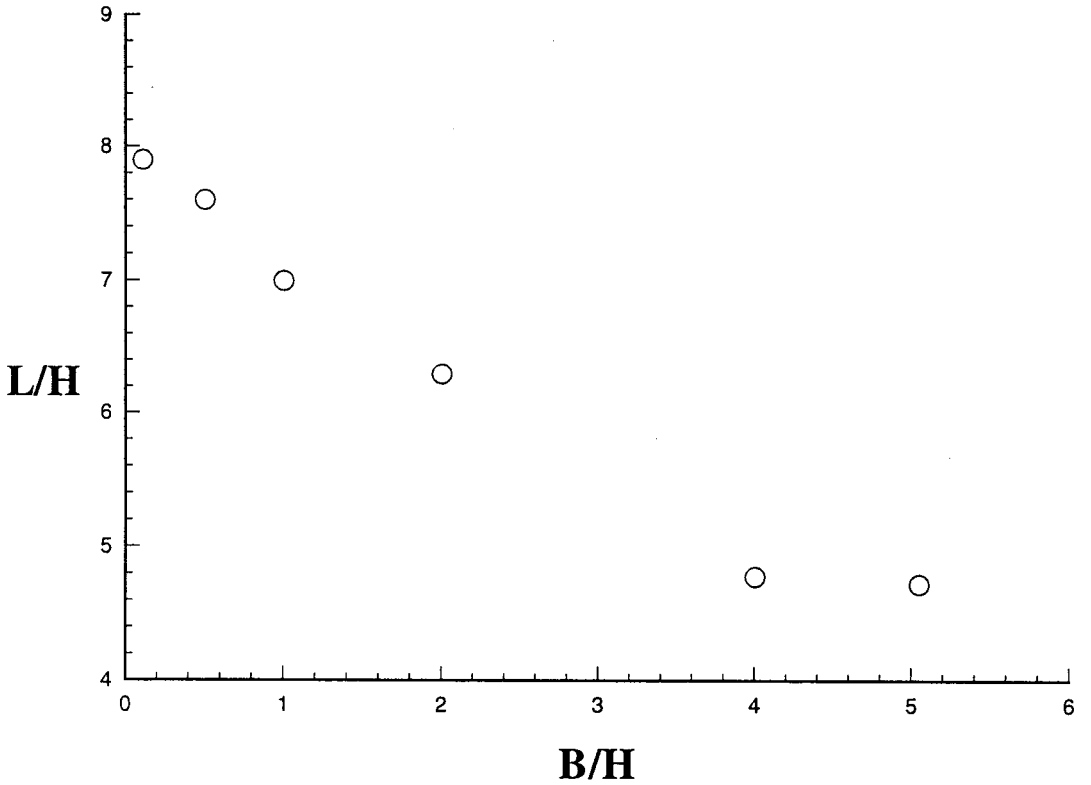

Figure 9. Length of recirculation region behind rib vs. B/H.

Wall static pressure distribution for flow over the rib is also obtained. The calculated wall static pressure distribution is expressed by the pressure coefficient, defined as

$$C_p = (P_w - P_c)/\frac{1}{2}\rho U_0^2,$$

here P_w is the bottom wall pressure and P_c is the reference pressure at the far upstream of the duct flow above the rib. Figure 10 presents the pressure coefficient distribution on the wall surface for various rib lengths. It can be seen that the distributions of the wall pressure coefficient are all the same in the rib's region upstream. It increases gradually and drops rapidly to a negative value at the rib's upstream corner owing to the blockage effect of the obstacle. The same distribution of wall static pressure indicates that the equal upstream recirculating lengths are formed for various cases of rib lengths. On the top surface of the obstacle, the pressure increases faster. When increasing the obstacle length it seems that the increase of the pressure is reduced and the leading-edge separation line is sucked toward the surface, resulting, therefore, in a quicker reattachment on the top surface, as it is shown for the case of $B/H = 4.0$. The wall pressure coefficient behind the rib remains constant for a distance and then increases smoothly to zero to recover the flow development along the flow direction. The predicted wall static pressure distributions for flows past a rib with varying lengths (Figure 10) also indicate the redevelopment rate of the flow behind the rib after reattachment. This finding reveals the faster recovery for the cases of $B/H > 2$ than that of $B/H < 2$. It may be stated that when reattachment on the top surface of the obstacle occurs, the flow development behind the rib recovers faster than that of the non-reattaching case.

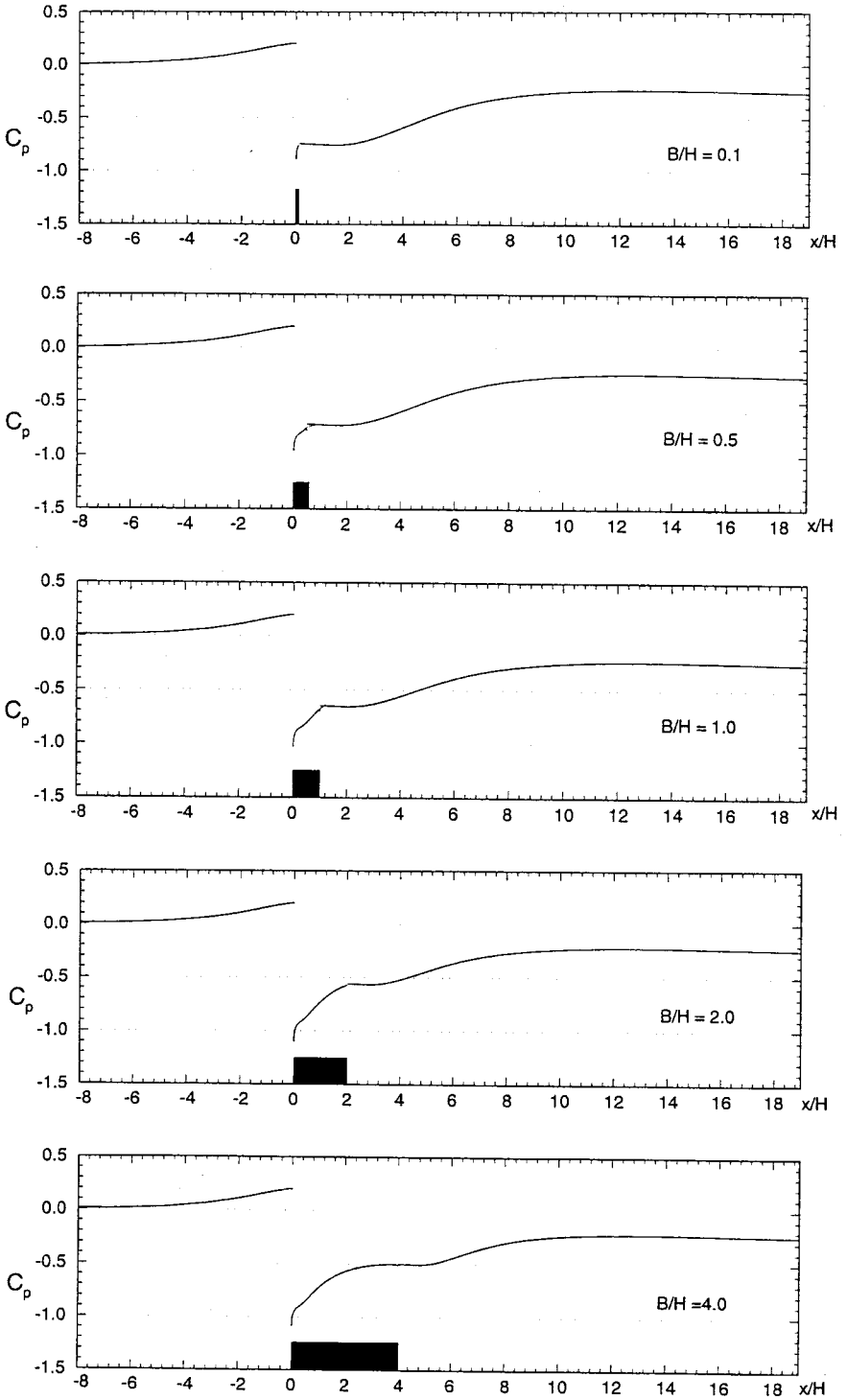

Figure 10. Wall static pressure distribution for flow over rib with varying length.

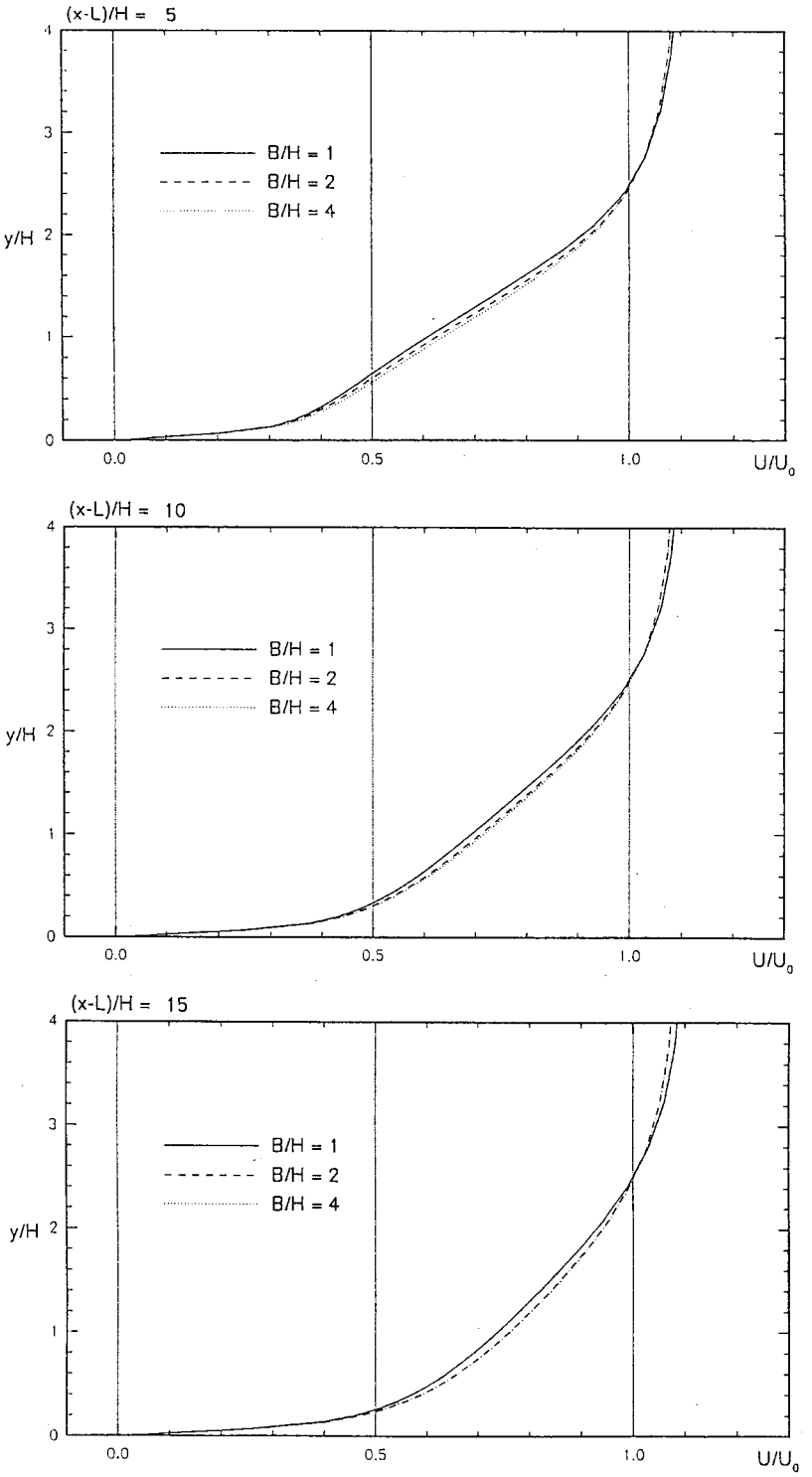

Figure 11. Mean velocity profiles at $X^*/H = 5$, 10 and 15.

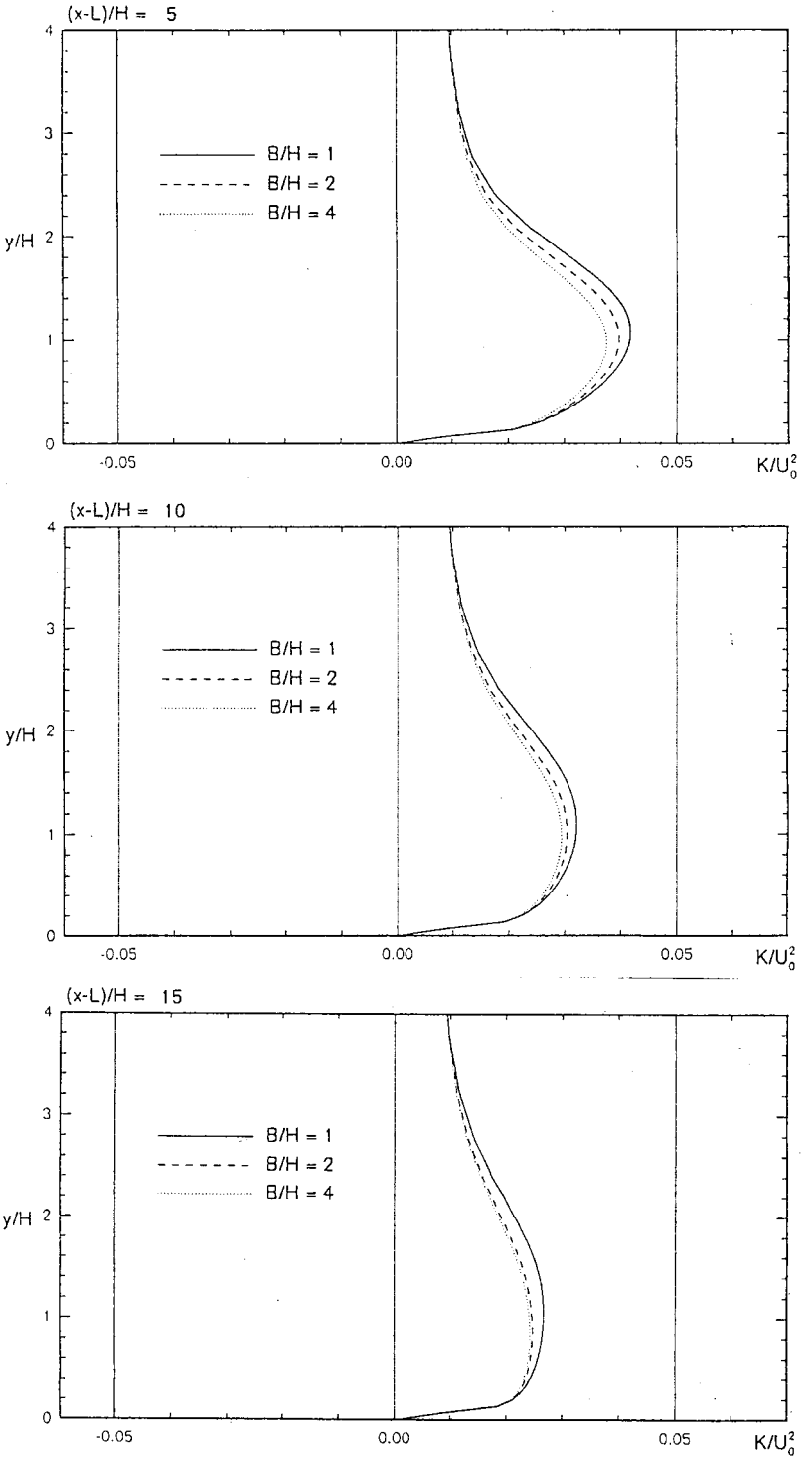

Figure 12. Turbulent kinetic energy profiles at $X^*/H = 5$, 10 and 15.

As mentioned previously, the flow separates from the upstream leading-edge and reattaches on the top surface of the rib or behind it depending on the value of the length to height ratio of the rib. The flow configuration of the region behind the rib of varying length after reattachment is also examined. Mean velocity and turbulence kinetic energy have been calculated at three stations downstream after reattachment from $X^*/H = 5$ to $X^*/H = 15$ for three different length to height ratios of the rib; $X^* = X - L$ is measured from the point of reattachment. Figure 11 shows velocity profiles at three stations of $X^*/H = 5$, 10 and 15 respectively for three lengths of the rib examined. It is observed that in cases of $B/H = 2$ and 4, at station $X^*/H = 10$, the mean velocity profiles for these two lengths coincide well with each other. Thus, it could be argued that, after the reattachment of the flow on the top of the rib occurs, the rate of flow recovery is almost the same. The corresponding profiles of turbulence kinetic energy are presented in Figure 12. At $X^*/H = 10$, the turbulence kinetic energies for cases of $B/H = 2.0$ and $B/H = 4.0$ nearly coincide with each other. At $X^*/H = 15$, it is seen that the mixing and spreading of the shear layer has resulted in a more uniform distribution of the turbulence kinetic energy. It can then be remarked that the redevelopment of the flow behind the rib after reattachment, at the same distance from reattachment, is seen to be different for cases of $B/H < 2$ and $B/H > 2$. It then depicts, as stated before, when reattachment on the top surface of the obstacle occurs, the flow development behind the rib after reattachment recovers faster than that of the non-reattaching case.

5. CONCLUSIONS

The turbulent flow past a surface-mounted two-dimensional rib with varying lengths has been numerically investigated. Compared with the previous studies, the use of the standard k–ε turbulence model in coupling with the near-wall treatment of the two-layer approach improved predictions of the mean velocities and Reynolds stresses near the wall region of the shear layer. The characteristics of the flow around surface-mounted obstacles depend appreciably on the length to height ratios of the obstacle. The flow separates from the upstream top corner of the obstacle and reattaches behind it. Increasing the obstacle length will cause the shear flow originating from the upstream edge of the obstacle to split twice at the reattachment points on top and behind the obstacle. The length of the recirculation region behind the obstacle was found to decrease linearly with increasing obstacle length and then to remain constant once reattachment on top of the obstacle occurred. The flow's redevelopment after reattachment at the same distance from reattachment is observed to be different for cases of varying length. The flow field behind the obstacle after reattachment recovers its boundary layer development more rapidly for the occurrence of reattachment on top of the obstacle than that behind it.

ACKNOWLEDGMENTS

This work was supported both by the National Science Council under Contract No. NSC84-0209-E001-012 and by the Institute of Physics, Academia Sinica, Taiwan, Republic of China.

REFERENCES

1. G. Bergeles and N. Athanassiadis, 'The flow past a surface-mounted obstacle', *ASME J. Fluids Eng.*, **105**, 461–463 (1983).
2. J. Antoniou and G. Bergeles, 'Development of the reattached flow behind surface-mounted two-dimensional prisms', *ASME J. Fluids Eng.*, **110**, 127–133 (1989).

3. S. Achraya, S. Dutta, T.A. Myrum and R.S. Baker, 'Turbulent flow past a surface-mounted two-dimensional rib', *ASME J. Fluids Eng.*, **116**, 238–246 (1994).
4. F. Durst and A.K. Rastogi, 'Turbulent flow over two-dimensional fences', *Turbul. Shear Flows*, **2**, 218–232 (1979).
5. R.W. Benodekar, A.J.H. Goddard, A.D. Gosman and R.I. Issa, 'Numerical prediction of turbulent flow over surface-mounted ribs', *AIAA J.*, **23**, 359–366 (1983).
6. V.C. Patal, W. Rodi and G. Scheuerer, 'Turbulence models for near-wall and low Reynolds number flows: a review', *AIAA J.*, **23**, 1308–1319 (1984).
7. V. Michelassi and T.H. Shih, 'Low Reynolds number two-equation modelling of turbulent flows', *NASA Tech. Memo. 104368*, 1991.
8. H.C. Chen and V.C. Patel, 'Near-wall turbulence models for complex flows including separation', *AIAA J.*, **26**, 641–648 (1988).
9. R.R. Hwang and Y.F. Peng, 'Effect of near-wall approach methods on the predictions of complex flows with flow separation and secondary reversed flow', *J. Chin. Inst. Eng.*, **17**, 421–428 (1994).
10. R.R. Hwang and Y.F. Peng, 'Computation of backward-facing step flows by a second-order Reynolds stress closure model', *Int. J. Numer. Methods Fluids*, **21**, 223–235 (1995).
11. B.E. Launder and D.B. Spalding, 'The numerical computation of turbulent flows', *Comput. Methods Appl. Mech. Eng.*, **3**, 269–289 (1974).
12. S.V. Patankar and D.B. Spalding, 'A calculation procedure for heat, mass, and momentum transfer in three-dimensional parabolic flows', *Int. J. Heat Mass Transf.*, **5**, 1878–1906 (1972).
13. J.P. Van Doormaal and G.D. Raithby, 'Enhancements of the simple method for predicting incompressible fluid flow', *Numer. Heat Transf.*, **7**, 147–163 (1984).
14. B.D. Nichols, C.W. Hirt and R.S. Hotchkiss, 'SOLA-VOF: a solution algorithm for transient fluid flow with multiple free boundaries', Los Alamos Scientific Laboratory Report, *LA-8355*, Los Alamos, NM, 1988.
15. W. Rodi, 'Experience with two-layer models combining the k–ε model with a one-equation model near the wall', *AIAA Paper 91-0216*, 29th Aerospace Sciences Meeting, January, Nevada, 1991.

